Identification of Rv3230c as the NADPH Oxidoreductase of a Two-Protein DesA3 Acyl-CoA Desaturase in *Mycobacterium tuberculosis* H37Rv[†]

Yong Chang and Brian G. Fox*

Biophysics Graduate Degree Program and Department of Biochemistry, University of Wisconsin, 433 Babcock Drive, Madison, Wisconsin 53706-1549

Received July 28, 2006; Revised Manuscript Received September 1, 2006

ABSTRACT: DesA3 is a membrane-bound stearoyl-CoA Δ^9-desaturase that produces oleic acid, a precursor of mycobacterial membrane phospholipids and triglycerides. The sequence of DesA3 is homologous with those of other membrane desaturases, including the presence of the eight-His motif proposed to bind the diiron center active site. This family of desaturases function as multicomponent complexes and thus require electron transfer proteins for efficient catalytic turnover. Here we present evidence that Rv3230c from *Mycobacterium tuberculosis* H37Rv is a biologically relevant electron transfer partner for DesA3 from the same pathogen. For these studies, Rv3230c was expressed as a partially soluble protein in *Escherichia coli*; recombinant DesA3 was expressed in *Mycobacterium smegmatis* as a catalytically active membrane protein. The addition of *E. coli* lysates containing Rv3230c to lysates of *M. smegmatis* expressing DesA3 gave strong conversion of [1-^{14}C]-18:0-CoA to [1-^{14}C]-*cis*-Δ^9-18:1-CoA and of [1-^{14}C]-16:0-CoA to [1-^{14}C]-*cis*-Δ^9-16:1-CoA. Both *M. tuberculosis* proteins were required for reconstitution of activity, as various combinations of control lysates lacking either Rv3230c or DesA3 gave minimal or no activity. Furthermore, the specificity of interaction between Rv3230c and DesA3 was implied by the inability of other related redox systems to substitute for Rv3230c. The reconstituted activity was dependent upon the presence of NADPH, could be saturated by increasing the amount of Rv3230c added, and was also sensitive to the salt concentration in the buffer. The results are consistent with the formation of a protein−protein complex, possibly with electrostatic character. This work defines a multiprotein, acyl-CoA desaturase complex from *M. tuberculosis* H37Rv to minimally consist of a soluble Rv3230c reductase and integral membrane DesA3 desaturase. Further implications of this finding relative to the properties of other multiprotein iron−enzyme complexes are discussed.

Mycobacterium tuberculosis is a human pathogen that causes one of the world's deadliest diseases, tuberculosis (TB).[1] Current estimates are that up to one-third of the world's population may be infected with *M. tuberculosis* and that more than 2 million people die from TB-related diseases each year (*1*−*4*). TB has resurged, in part due to the appearance of multiple-drug-resistant strains. Consequently, the development of new drugs and the re-examination of drugs formerly deemed effective have become major focuses of worldwide TB research (*3*−*5*). This intense effort has included genome sequencing (*6*), proteome functional analysis by microarray approaches (*7*−*11*), the TB Protein Structure Initiative (*12*; http://www.doe-mbi.ucla.edu/TB/), and many other studies of regulatory, metabolic, and enzymatic pathways in pathogenic mycobacteria.

One discovery arising from the *M. tuberculosis* genome sequence annotation was the predominance of genes involved in lipid metabolism (*6*, *13*, *14*). This likely reflects the importance of mycolic acid to mycobacterial physiology. Mycolic acid is a waxlike substance assembled from long chain fatty acids that is incorporated into the outer cell wall and helps to protect mycobacteria from desiccation, water-soluble antibiotics, macrophage attack, and other ameliorative agents (*15*). Thus, disruption of mycolic acid biosynthesis is recognized as a viable strategy for TB treatment.

The mechanisms used to synthesize mycolic acids are not clear at present. Long chain fatty acids containing position-specific double bonds are required building blocks, but the biosynthetic origins of the inserted double bonds have not been clearly established. For example, chain elongation of enoyl-ACP intermediates during fatty acid biosynthesis has been proposed to provide the necessary precursors (*16*). Alternatively, multiprotein diiron enzymes such as those found in humans and other eukaryotes might also catalyze the O_2-dependent and position-specific insertion of the required double bonds (*13*). In this regard, the genome sequence of *M. tuberculosis* and related pathogens has revealed the presence of three O_2-dependent desaturase-like genes (*6*, *13*). Among these three genes, *rv0824c* (encoding DesA1) and *rv1094* (encoding DesA2) are annotated to be homologues of the soluble acyl-ACP desaturases found in plants (*6*, *17*, *18*); the X-ray structure of DesA2 supports the structural assignment (*19*). Furthermore, alkaline phos-

[†] This work was supported by National Institutes of Health Grant R01 GM-50853 to B.G.F.

* To whom correspondence should be addressed: Department of Biochemistry, University of Wisconsin, 433 Babcock Dr., Madison, WI 53706. Telephone: (608) 262-9708. Fax: (608) 262-3453. E-mail: bgfox@biochem.wisc.edu.

[1] Abbreviations: AlkB, alkane ω-hydroxylase; DesA3, product of *M. tuberculosis* H37Rv gene *rv3229c*, a stearoyl-CoA Δ^9-desaturase; Rv3230c, product of *M. tuberculosis* H37Rv gene *rv3230c*, a proposed DesA3:NADPH oxidoreductase; SCD, stearoyl-CoA Δ^9-desaturase; TB, tuberculosis.

10.1021/bi0615285 CCC: $33.50
Published on Web 10/24/2006

Table 1: Bacterial Strains and DNA Constructs Used in This Study

	relevant characteristics	source or reference
strains		
E. coli strain TOP10	F$^-$ *mcr*A (*mrr-hsd*RMS-*mcr*BC) 80*lac*ZM15 *lac*X74 *rec*A1 *ara*D139 (*ara-leu*)7697 *gal*U *gal*K *rps*L(Str^R) *end*A1 *nup*G {P3: Kan^R, Amp^R (Amber), Tet^R (amber)}	Invitrogen
E. coli Rosetta2	F$^-$ *ompT hsdS*$_B$(r_B^- m_B^-) *gal dcm* pRARE2 (*cam*^{R} and tRNA genes *argU, argW, argX, ileX, glyT, leuW, proL, metT, thrT, tyrU, and thrU*)	Novagen
M. smegmatis mc^{2}155	mycobacterial expression host with a high transformation efficiency	ATCC 700084 (*68*)
plasmids		
pQE80	commercially available *E. coli* expression vector	Qiagen
pVV16	shuttle vector and mycobacterial expression vector	(*29*)
pQE80-Rv3230c	*rv3230c* in pQE80	this work
pVV16-DesA3	*desA3* in pVV16	this work

phatase fusion studies with DesA1 (*20*, *21*) and nuclease fusion studies with DesA2 (*22*) indicate that these two mycobacterial proteins may be transported to the extracellular space. Indeed, DesA1 is a major surface antigen of mycobacteria in infected human patients (*21*). Still, the true biological functions of these two mycobacterial proteins have not yet been established.

In contrast to the uncertainty regarding the function of DesA1 and DesA2, DesA3 (encoded by the *rv3229c* gene) is a membrane enzyme demonstrated to have stearoyl-CoA Δ^9-desaturase activity (*5*). One product of this reaction, oleic acid, is an essential constituent of mycobacterial membrane phospholipids and triglycerides (*5*, *23*−*25*). Thus, DesA3 is suggested to be a target of isoxyl (also known as thiocarlide), an anti-tuberculosis drug that inhibits the synthesis of oleic and mycolic acids (*5*).

DesA3 shares the conserved eight-His motif found in membrane acyl-lipid and acyl-CoA desaturases and in the related bacterial membrane enzymes alkane hydroxylase and xylene monooxygenase (*5*, *26*−*28*). Via this assessment, DesA3 is likely to be an integral membrane diiron enzyme. Since these other desaturases and hydroxylases require one or more electron transfer partners to pass two electrons from either NADH or NADPH to the active site diiron center, the identification of the electron transfer partner(s) for DesA3 would help to advance the understanding of mycobacterial lipid metabolism. In this work, we provide biochemical evidence that Rv3230c, encoded by the *rv3230c* gene, is the biologically relevant electron transfer partner for DesA3, encoded by the *rv3229c* gene. Some implications of this assignment are considered.

EXPERIMENTAL PROCEDURES

DNA and Plasmid Reagents. Table 1 lists the bacterial strains and plasmids used in this work. Total genomic DNA of *M. tuberculosis* H37Rv was obtained from the TB Research Materials Facility at Colorado State University (Fort Collins, CO) (J. Belisle, Director, NIH NIAD NO1AI75320). This material was used to clone *rv3230c* and *rv3229c* (encoding DesA3) by PCR methods. Pfu DNA polymerase was from Stratagene (La Jolla, CA). Oligonucleotide primers were obtained from Integrated DNA Technologies, Inc. (Coralville, IA). *Escherichia coli* strain TOP10 (Invitrogen, Carlsbad, CA) was used for all cloning work. The pQE80 expression vector (Qiagen, Valencia, CA) was used to express Rv3230c in *E. coli*. The pVV16 shuttle/expression vector (*29*) was used to express DesA3 as a C-terminal His_6-tagged fusion protein under the control of the transcriptional and translational signals of the hsp60 promoter in *Mycobacterium smegmatis* (ATCC 700084). Big Dye DNA sequencing (Applied Biosystems, Foster City, CA; performed by the University of Wisconsin Biotechnology Center) was used to verify the coding sequence of the expression plasmids.

Cloning of Rv3230c. The *rv3230c* gene was amplified by PCR using the primers 5′-cgggGTACCatcgagggaaggatgag-caagaaacacacgac-3′ and 5′-cccAAGCTTctagatgtccagcacg-caatcac-3′. The KpnI and HindIII restriction sites are indicated in capital letters. The PCR mixture contained 10% dimethyl sulfoxide and consisted of 30 cycles of melt, anneal, and extend at temperatures of 94, 55, and 72 °C, respectively. The resulting DNA fragment was purified by gel electrophoresis and extracted using a QIAquik gel extraction kit (Qiagen). The PCR product was digested with KpnI and HindIII and ligated into a similarly digested pQE80 vector to create expression vector pQE80-Rv3230c. *E. coli* TOP10 pQE80-Rv3230c transformants were cultured on either Luria-Bertani broth or agar medium, each containing 100 μg/mL ampicillin. Plasmids isolated from these cells were used to verify the sequence of the PCR-cloned gene.

Expression of Rv3230c. E. coli Rosetta2 (Novagen, Madison, WI) transformed with pQE80-Rv3230c was used for expression studies. The transformed strain was cultured on either Terrific Broth or Luria-Bertani agar medium containing 34 μg/mL chloramphenicol and 100 μg/mL ampicillin. Expression of Rv3230c was induced by addition of IPTG to a final concentration of 0.5 mM and continued overnight at 16 °C. The cells harvested from a 2 L culture (∼5 g) were washed once in 20 mM NaH_2PO_4 (pH 7.2) containing 150 mM NaCl and resuspended in the same buffer at a composition of 1 g of wet cell paste per 2 mL of buffer.

Fractionation of Rv3230c. The cell suspension was sonicated for a total of 150 s using a duty cycle of 15 s on and 45 s off (Fisher model 550 sonic dismembrator, $^1/_8$ in. horn). During sonication, the temperature of the cell suspension was kept below 10 °C by placing the beaker in an ice/water bath containing NaCl. The sonicated cell suspension was centrifuged at 27000*g* for 30 min, and the supernatant fraction was retained for activity assays. The cell lysates were analyzed for total expression and the presence of Rv3230c in the soluble fraction by Western blotting with primary mouse anti-His-tagged antibody (Novagen) and SDS−PAGE. Samples were prepared and fractionated for SDS−PAGE using approaches developed for high-throughput structural genomics studies (*30*). For the immunoprecipitation, the lysate was treated with antibody and then the antigen−

antibody complex was precipitated by addition of Protein G-linked Sepharose resin (Amersham, Piscataway, NJ). The precipitated sample of Rv3230c was purified by SDS−PAGE and further analyzed by trypsin digestion and mass spectrometry at the University of Wisconsin Biotechnology Center.

Cloning of DesA3. The *rv3229c* gene (encoding DesA3) was amplified using the primers 5′-gggaattcCATATGgcgatcactgacgtcgacgtattcgcg-3′ and 5′-cccAAGCTTggctgccagatcgtcgggttcgg-3′. The NdeI and HindIII restriction sites are indicated in capital letters. The PCR mixture contained 10% dimethyl sulfoxide and consisted of 30 cycles of melt, anneal, and extend at temperatures of 94, 55, and 72 °C, respectively. The resulting DNA fragments were purified by gel electrophoresis and extracted using a QIAquik gel extraction kit. The PCR product was digested with NdeI and HindIII and ligated into the similarly digested pVV16 to create expression vector pVV16-DesA3. *E. coli* TOP10 pVV16-DesA3 transformants were cultured on either Luria-Bertani broth or agar medium containing 50 μg/mL kanamycin. Plasmids isolated from these cells were used to verify the sequence of the PCR-cloned gene.

Expression of DesA3. M. smegmatis (ATCC 700084) was transformed by electroporation with either pVV16-DesA3 or pVV16 containing no insert. These transformants were maintained on either Middlebrook 7H10 agar medium or Middlebrook 7H9 broth enriched with Middlebrook OADC (oleic acid/albumin/dextrose/catalase, Becton Dickinson, Spark, MD) and 20 μg/mL kanamycin. The expression studies were performed in 2 L of the enriched medium. DesA3 was constitutively expressed at 37 °C. The cells were grown for ∼38 h, harvested by centrifugation, and washed once in 20 mM NaH_2PO_4 (pH 7.2) containing 500 mM NaCl.

Preparation of M. smegmatis Lysate. The cell paste was resuspended in the wash buffer at a composition of 1 g of wet cell paste per 2 mL of buffer. The cell suspension was sonicated for a total of 480 s using a duty cycle of 15 s on and 45 s off with the temperature of the suspension kept below 10 °C. A fraction of the total lysate was retained for assays and other analyses, and the remainder was centrifuged at 27000*g* for 30 min to separate the supernatant and the pellet fractions. The soluble fraction was removed, and the pellet fraction was resuspended in the same volume as the total cell lysate subjected to centrifugation. The three samples were then treated with the same amount of 50 mM Tris-HCl (pH 7.4) containing 150 mM NaCl, 1 mM phenylmethanesulfonyl fluoride, 1 mM EDTA, 1% Triton X-100, 1% sodium deoxycholate, and 0.1% SDS. For immunoprecipitation, the expressed DesA3 was treated with the primary mouse anti-His-tagged antibody and analyzed by trypsin digestion and mass spectrometry as described for Rv3230c.

Desaturation Assay. Radioactive fatty acyl-CoAs were obtained from American Radiolabeled Chemicals (St. Louis, MO). The DesA3 activity assay was similar to an SCD activity assay (*31*). The reaction mixture contained 20 mM potassium phosphate and 150−250 mM NaCl in a total reaction volume of 200 μL. Aliquots (20 μL) of the *M. smegmatis* pVV16 or pVV16-DesA3 total lysate, supernatant, or pellet fractions were added in various combinations with aliquots (15 μL) of the supernatant fraction prepared from either *E. coli* pQE80 or pQE80-Rv3230c. The reaction was initiated by addition of 0.4 μmol of NADPH, 6 nmol of stearoyl-CoA, 0.03 μCi of [1-^{14}C]stearoyl-CoA, and 0.2 nmol of FAD in a combined volume of 200 μL. The reaction mixture was incubated at 37 °C for 1 h and the reaction stopped by the addition of 200 μL of 2.5 M KOH in ethanol. The mixture was heated at 80 °C for 1 h and acidified by the addition of 280 μL of formic acid. The saponified fatty acids were extracted with 700 μL of hexane; 200 μL of the extract was evaporated to dryness, resuspended in 50 μL of hexane, and separated into saturated and unsaturated acids on a 10% $AgNO_3$-impregnated thin-layer chromatography plate using a chloroform/methanol/acetic acid/water mixture (90:8:1:0.8) as the developing solvent. Radioactivity was counted by phosphorimaging using a Packard Instant Imager (Packard, Meriden, CT) for 30−60 min. Samples prepared in this manner gave ∼200 total imager units for the major radioactive bands that were detected, which is within the linear response range of the instrument. Reactions performed with stearoyl-CoA were also assessed by thin-layer chromatography as described above, and the individual bands were extracted from the plate, methylated, and analyzed by GC−MS to determine fatty acid content (*32*). For unsaturated fatty acids, the position of double bonds was determined as previously described (*33*).

For studies of the Rv3230c dependence of the reaction, different volumes of an *E. coli* pQE80-Rv3230c lysate containing Rv3230c were added to provide 0−1.28 mg of total protein. For studies of the salt dependence of the reaction, the NaCl concentration in the buffer was varied from 1.3 mM (no additional NaCl added) to 1000 mM. For studies of the pyridine nucleotide dependence, either NADH or NADPH was added in the concentration range from 0 to 2 mM. For studies of the flavin dependence, either FAD or FMN was added in the concentration range from 0 to 16 μM. For studies of the ability of other reductases to substitute for Rv3230c, toluene 4-monooxygenase reductase (*34*, *35*) was added in the concentration range from 0 to 1 μM and NADH replaced NADPH. In addition, assays were performed with *Anabaena* [2Fe-2S] ferredoxin and corn root ferredoxin reductase, mimicking the method and two-protein electron transfer chain used to assay plant stearoyl-ACP Δ^9-desaturase (*18*).

Other Analyses. The primary sequences of proteins related to Rv3230c and DesA3 were obtained from a BLASTP search initiated at http://www.ncbi.nlm.nih.gov/BLAST/. Operon prediction (*36*) was obtained from The Institute for Genomic Research website (http://www.tigr.org/tdb/). PFAM searches and protein domain assignments (*37*) were performed using the Washington University mirror site (http://pfam.wustl.edu). Kyte−Doolittle hydropathy analysis (*38*) was performed using Protean (DNASTAR, Madison, WI). The TMHMM prediction program (*39*, *40*; http://www.cbs.dtu.dk/services/TMHMM-2.0) was also used to analyze the putative transmembrane topologies. Multiple-sequence alignments were produced from CLUSTALW (*41*) with default parameters using MegAlign (DNASTAR). SWISS-MODEL (*37*) was used for threading of the Rv3230c primary sequence to the structure of phthalate dioxygenase reductase [Protein Data Bank entry 2PIA (*42*)].

RESULTS

Bioinformatics Analysis of Rv3230c. In the *M. tuberculosis* H37Rv genome, the *rv3230c* gene is located immediately

Table 2: Correlation of the Fold Change in the Level of Expression of DesA3 and Rv3230c from Genome-Level Studies of *M. tuberculosis*[a]

growth condition	*rv3329c (desA3)*	*rv3230c*
nutrient starvation for 4 h	−8.55	−3.21
nutrient starvation for 24 h	−5.41	−2.39
nutrient starvation for 96 h	−6.62	−3.08
palmitic acid (0.05 mM)	11.6	2.6
H_2O_2 (5 mM)	7.2	6.2

[a] Results selected from expression studies undertaken by others (*8*, *9*).

before the *rv3229c* gene. *rv3230c* was annotated to encode a putative oxidoreductase, while *rv3229c* was annotated to encode a membrane desaturase. Similar gene pairs are found in other genomes, notably including the pathogens *M. tuberculosis* CDC1551, *Mycobacterium bovis* AF2122/97, *Mycobacterium avium paratuberculosis*, and *Corynebacterium diphtheria*. The annotation of *rv3229c* was previously confirmed by heterologous expression and measurement of stearoyl-CoA desaturase activity (*5*).

Previous operon prediction analyses indicated a high probability that *rv3230c* and *rv3329c* would be part of an operon (http://www.tigr.org/tdb/ and http://www.doe-mbi.ucla.edu/~strong/map/) and that numerous other mycobacterial ferredoxins and oxidoreductases would not be coexpressed with *rv3229c*. Consistent with this assessment, genome-level expression studies (*8*, *9*) revealed the coordinated expression of *rv3230c* and *rv3229c* under a variety of growth conditions (Table 2). Taken together, these results suggested that *rv3230c* and *rv3329c* would be expressed together and thus plausibly have a functional relationship.

Protein family analysis indicated that Rv3230c, the putative oxidoreductase encoded by the *rv3230c* gene, consists of flavin binding, NAD binding, and [2Fe-2S] ferredoxin domains. Figure 1 shows a schematic representation of this linkage of redox domains and includes comparable representations of the domains of other oxidoreductase complexes considered in this work. The other oxidoreductases shown in Figure 1 catalyze electron transfer reactions between NAD(P)H and iron-containing enzymes such as the *cis*-diol-forming aromatic ring dioxygenases (*43*−*45*), the bacterial diiron center hydroxylases (*34*, *46*), and plant acyl-ACP desaturases (*17*). Among the three-domain reductases, phthalate dioxygenase reductase [2PIA (*42*)] and benzoate 1,2-dioxygenase reductase [1KPH (*47*)] provide representative three-domain structures. The domain arrangement in Rv3230c matches that of phthalate dioxygenase reductase (*42*), with the flavin binding domain located at the N-terminus and the [2Fe-2S] ferredoxin domain located at the C-terminus. Rv3230c and phthalate dioxygenase reductase are ~23% identical in sequence. Rv3230c also differs from other related reductases as it has a calculated pI of 9.4, as compared to pI values of 5.9 for phthalate dioxygenase reductase, 5.1 for toluene 4-monooxygenase reductase, 4.1 for *Anabaena* [2Fe-2S] ferredoxin, and 8.1 for corn root ferredoxin reductase. For comparison, the individual FAD and NAD binding domains (residues 63−226) and [2Fe-2S] ferredoxin domain (residues 300−380) from Rv3230c have pI values of 10.0 and 5.5, respectively.

Bioinformatics Analysis of DesA3. Kyte−Doolittle hydropathy analysis was previously used to deduce the positions of four long stretches of hydrophobic residues in rat SCD that might act as transmembrane helices (*26*). Figure 2 shows a combination of this analysis and the location of the eight-His motif (*26*) for human SCD and bacterial AlkB, two representative diiron enzymes known to be integral membrane proteins, along with a comparable analysis of DesA3. This analysis predicts that SCD will have four transmembrane regions (Figure 2A) and also predicts that AlkB may have up to six transmembrane regions (Figure 2B). By comparison, the Kyte−Doolittle analysis shown in Figure 2 predicts that DesA3 may have only three hydrophobic sequences of 18 residues, long enough to cross the cell membrane.

As a further evaluation of membrane protein topology, the TMHMM analysis of SCD and AlkB, also shown in Figure 2, still predicts four and six transmembrane helices, respectively (red lines). Figure 2 also shows the probability that a given residue position may be on the interior of the membrane (blue line) or on the exterior (green line) according to the TMHMM analysis. In contrast to the prediction with SCD and AlkB, the TMHMM analysis of DesA3 predicted only one likely transmembrane helix motif. Thus, while DesA3 appears to retain the eight-His motif associated with other membrane diiron enzymes, current bioinformatics analyses do not recognize the topology predicted in the other known integral membrane enzymes, including the spacing and length of putative transmembrane hydrophobic sequences, the relative location of the putative eight-His metal binding motif, and the disposition of the C-terminal region relative to the interior surface of the membrane. Others have noted the specific residue differences near the eight-His motif (*5*).

Expression Studies. Rv3230c was expressed in *E. coli* Rosetta2 as a fusion to an N-terminal His_6 tag. Figure 3A shows that the expressed Rv3230c could be detected by use of the anti-His tag antibody and denaturing SDS−PAGE. Total expressed Rv3230c partitioned between the soluble and pellet fractions after centrifugation. Overall, the expressed protein was only sparingly soluble under the expression conditions that were used. Figure 4A shows the primary sequence of Rv3230c, while Table 3 shows the results of tryptic digest MALDI-MS of Rv3230c purified by immunoprecipitation using an anti-His_6 tag antibody. The tryptic digest work revealed five peptides, indicated with bold type in Figure 4A (note that trypsin cleaves Rv3230c between Arg355 and Met356), whose masses closely match the predicted Rv3230c digestion profile. These five peptides represent 28% of the complete sequence. Among the five peptides, the primary sequences of two peptides were confirmed by further MS/MS sequencing, and these two peptides are indicated with bold and italic type in Figure 4A. These positive results confirm that Rv3230c was expressed in *E. coli*.

A pVV16 mycobacterial expression vector (*29*) was used to express DesA3 containing a C-terminal His tag in *M. smegmatis*. For screening purposes, an anti-His tag antibody was used to localize DesA3. Figure 3B shows that the majority of the total expressed DesA3 was in the pellet fraction, while the supernatant fraction contained only a small amount of antibody-reactive protein. Figure 4B shows the primary sequence of DesA3. Table 3 shows the results of tryptic digest MALDI-MS of the DesA3 purified by immu-

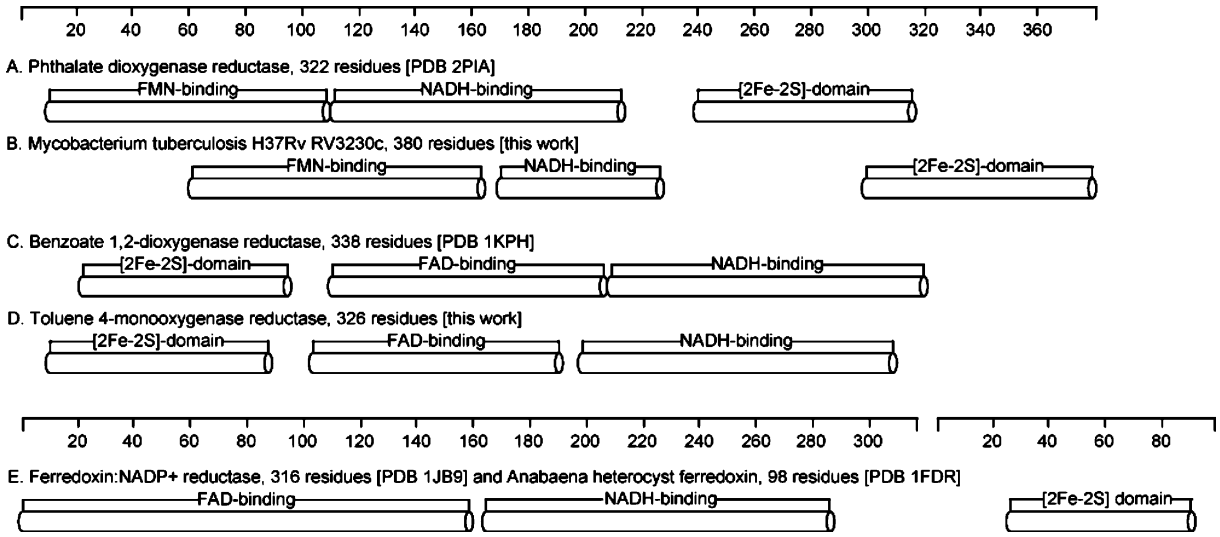

FIGURE 1: Schematic representation of the domain structure of Rv3230c and related oxidoreductases with different arrangements of flavin binding, NAD binding, and [2Fe-2S] ferredoxin domains: (A) phthalate dioxygenase reductase, (B) Rv3230c, (C) benzoate 1,2-dioxygenase reductase, (D) toluene 4-monooxygenase reductase, and (E) corn root ferredoxin reductase and *Anabaena* [2Fe-2S] ferredoxin.

noprecipitation using an anti-His_6 tag antibody and denaturing SDS−PAGE. This work revealed nine peptides (22% of the complete protein) with masses that closely matched the predicted DesA3 digestion profile, thus confirming that the expressed membrane protein was DesA3.

Reconstitution of DesA3 Activity. Figure 5 and Table 4 show results from stearoyl-CoA Δ^9-desaturase assays using various combinations of the total cell lysates, supernatants, and pellet fractions of *M. smegmatis* and the supernatant fractions of *E. coli* Rosetta2.

Figure 5A and Table 4 show results of control experiments using lysates prepared from *M. smegmatis* transformed with pVV16 lacking a gene insert. For each experiment, the total cell lysate, the soluble fraction, and the resuspended pellet fraction were evaluated. The addition of buffer, a lysate prepared from *E. coli* Rosetta2 transformed with an empty pQE80 vector or a lysate prepared from *E. coli* Rosetta2 pQE80-Rv3230c, gave little or no significant conversion of 18:0-CoA to 18:1-CoA above background. This shows that either *M. smegmatis* or *E. coli* as grown for this study does not have a detectable 18:0-CoA Δ^9-desaturase activity. Likewise, Figure 5B shows that the total pVV16-DesA3 lysate supplemented with either buffer alone or the control lysate from *E. coli* Rosetta2 pQE80 gave similarly low but detectable activity (lanes 1 and 4).

When the *M. smegmatis* pVV16-DesA3 total lysate, supernatant, and pellet fractions were treated with the lysate from *E. coli* Rosetta2 pQE80-Rv3230c (Figure 5B, lanes 7−9, and Table 4), an increase in the extent of conversion of 18:0-CoA to 18:1-CoA was observed from all three fractions as compared to the addition of the control lysate (lanes 4−6). GC−MS analysis of the product band showed that a Δ^9 position double bond was present, which was consistent with the migration position when compared to a *cis*-Δ^9-18:1 standard. For the combination of the pellet fraction and the pQE80-Rv3230c lysate, a ~10-fold increase in activity was obtained. When the pVV16-DesA3 pellet fraction and Rv3230c supernatant were reacted with 16:0-CoA, the major product of the reaction was *cis*-Δ^9-16:1 as determined by thin-layer chromatography.

In other experiments (data not shown), the reconstituted desaturation activity was best in buffer containing ~150−500 mM NaCl but decreased above this salt concentration. This result suggests an ionic contribution to solubility, stability, or complex formation. Furthermore, the addition of FAD above 1 μM approximately doubled the desaturation activity, while the addition of FMN provided an only slight stimulation, suggesting that Rv3230c may use FAD as a cofactor. As compared with NADPH, NADH did not stimulate the desaturation activity in the concentration range from 0 to 2 mM, indicating Rv3230c is specific for the use of NADPH. DesA3 was also abundantly expressed as a C-terminal fusion with maltose binding protein in *E. coli* Rosetta2 and appeared in the pellet fraction. However, lysates prepared from these cells gave no NADPH-dependent conversion of 18:0-CoA, either alone or when supplemented with the *E. coli* supernatant containing Rv3230c.

Saturation of DesA3 Activity by Rv3230c. To further investigate the specificity of the reaction of Rv3230c with DesA3, different volumes of the lysate containing Rv3230c were added to the pellet fraction prepared from *M. smegmatis* pVV16-DesA3. Figure 6 shows that increasing the amount of control lysate prepared from the *E. coli* pQE80 empty vector did not increase the amount of 18:1-CoA formed. In contrast, increasing amounts of *E. coli* lysate containing Rv3230c stimulated production of 18:1-CoA to a maximal level, consistent with saturation of a binding interaction. However, further addition of the Rv3230c lysate decreased the amount of 18:1-CoA that was produced. For example, with the addition of more than 1 mg of total protein from the Rv3230c lysate, the desaturation reaction was almost completely blocked. As a different test of the specificity of the reaction, addition of the purified toluene 4-monooxygenase reductase (domain arrangement similar to that of benzoate 1,2-dioxygenase reductase, 1KPH; see Figure 1) in the concentration range of 0−1 μM did not complement DesA3 activity. Likewise, the use of *Anabaena* [2Fe-2S] ferredoxin and corn root ferredoxin reductase [a two-protein electron complex (*18*); see Figure 1] did not complement DesA3 activity.

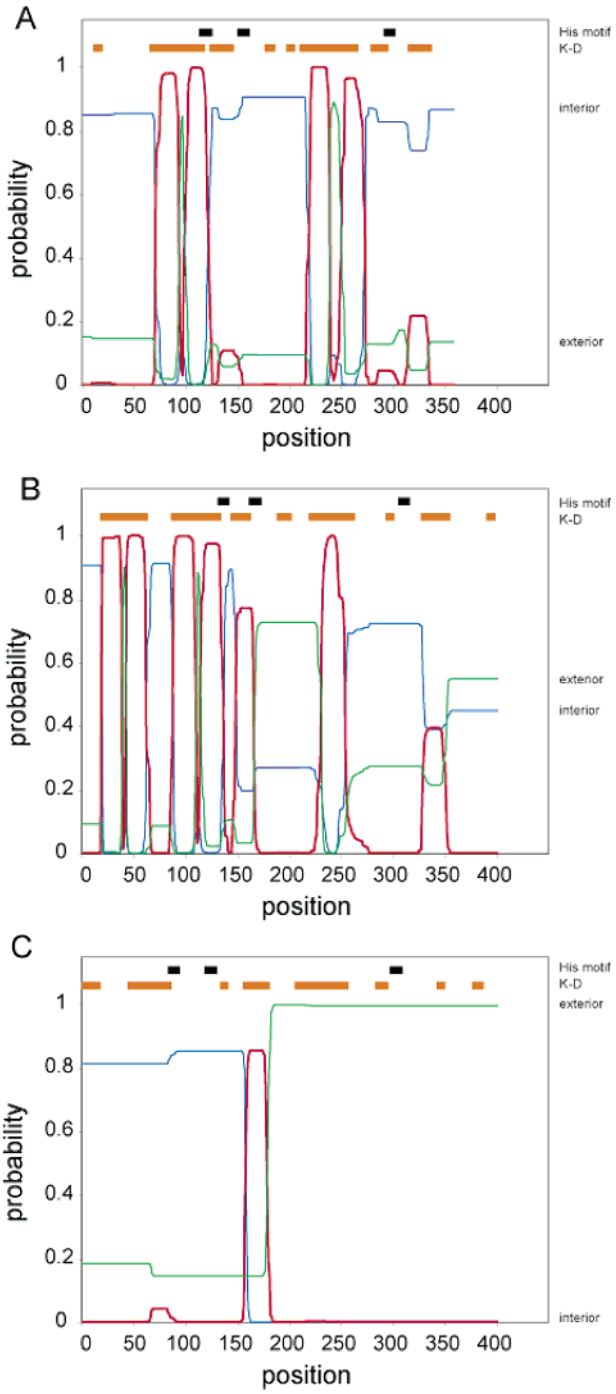

FIGURE 2: Results of a bioinformatics analysis of membrane protein structure: (A) human SCD isoform 1, 359 residues long, GenBank entry 2190404, (B) AlkB from *Pseudomonas putida* Gpo1, 401 residues long, GenBank entry 113639, and (C) DesA3 from *M. tuberculosis* H37Rv, 427 residues long, GenBank entry 57117078. The red lines show the probability that the residue is part of a transmembrane sequence; the blue lines show the probability that a given residue position is on the interior of the membrane, and the green lines show the probability that the residue position is on the exterior. Each analysis includes the location of the diagnostic eight-His metal binding motif (His motif, black boxes) and long hydrophobic stretches predicted by Kyte−Doolittle hydropathy analyses (KD, orange boxes).

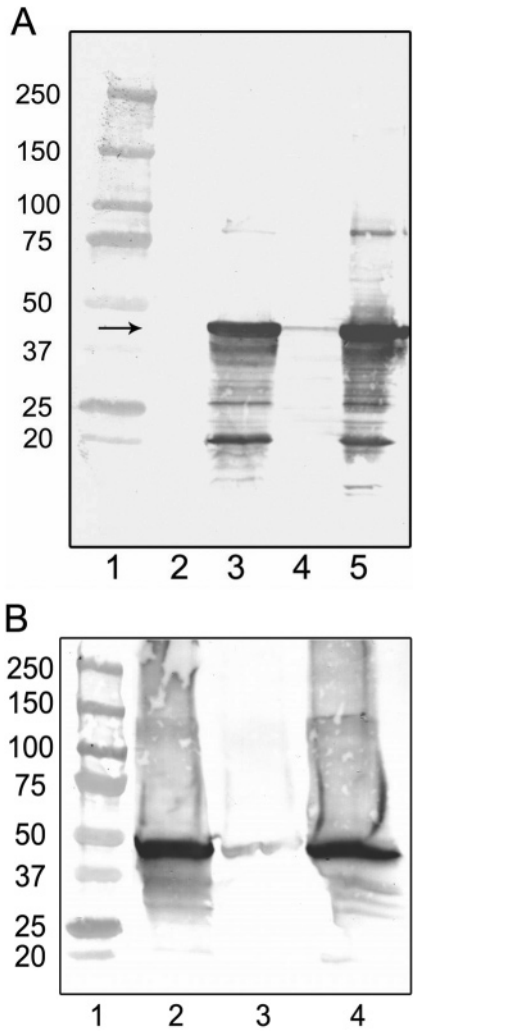

FIGURE 3: Protein expression detected by Western blotting. (A) Expression of Rv3230c in *E. coli* Rosetta2. Lane 1 contained molecular weight markers, lane 2 a sample taken immediately before induction, lane 3 the induced sample, lane 4 the supernatant fraction obtained from the induced cells, and lane 5 the pellet fraction of the lysate. (B) Localization of DesA3 expressed in *M. smegmatis*. An anti-His_6 tag antibody was used to detect recombinant DesA3 containing a C-terminal His_6 tag. Lane 1 contained molecular weight markers, lane 2 the total cellular lysate, lane 3 the supernatant fraction, and lane 4 the resuspended pellet fraction.

DISCUSSION

The results presented here arise from the heterologous expression of DesA3 in *M. smegmatis*, which yields a catalytically active desaturase that is located in the membrane fraction. In this work, we have further shown that the combination of an *E. coli* lysate containing recombinant Rv3230c and a *M. smegmatis* pellet fraction containing DesA3 gives rise to a substantial enhancement of desaturase activity. On the basis of this result, we propose that DesA3 and Rv3230c represent a functional two-protein desaturase complex from *M. tuberculosis* H37Rv. Some of the implications of this finding are discussed below.

Topology of Membrane Desaturases. DesA3 shares the eight-His motif of the membrane acyl-lipid and acyl-CoA desaturases, the bacterial alkane and xylene monooxygenases, and other O_2-dependent enzymes (*5*, *26*−*28*). Kyte−Doolittle analysis of these other proteins revealed the presence of multiple hydrophobic sequences that may span the cellular membrane (*26*). Likewise, previous Kyte−Doolittle hydropathy analysis suggested that DesA3 might contain up to three hydrophobic domains (*5*). For comparison, TMHMM analysis predicted four transmembrane helices for SCD and six transmembrane helices for AlkB but predicted no putative

A. Rv3230c

```
   1   MRGSHHHHHH GSACELGTIE GRskkhttln
  31   asiidtrrpt vagadrHPGW HALRKiaarI
  61   TTPLLPDDYL HLANPLWSAR elrgrilgvr
  91   retedsatlf ikpgwgfsfd yqpgqyigig
 121   llvdgrwrwr syslsspaa sgsarmvtvt
 151   vkampegfls thlvagvkpg tivrlaapqg
 181   nfvlpdpapp lilfltagsg itpvmsmlrt
 211   lvrrNQITDV VHLHSAPTAA DVMFGAELAA
 241   LAADHPGYRl svretraqgr ldltrigqqv
 271   pdwrerqtwa cgpegvlnqa dkvwssagas
 301   drlhlerfav sktapagagg tvtfarsgks
 331   vAADAATSLM DAGEGAGVQL PFGCRMGICQ
 361   SCVVDLVEGH Vrdlrtgqrh epgtrvqtcv
 391   saasgdcvld i
```

B. Rv3229c

```
   1   maitdvdvfa hltdadienl aaeldairrd
  31   veesrgerda ryirrtiaaq rALEVSGRLL
  61   LAGSSRrlaw wtgaltlgva kiienmeigh
  91   nvmhgqwdwm ndpeihsstw ewdmsgsskh
 121   wrYTHNFVHH Kytnilgmdd dvgygmlrvt
 151   rdqrwkryni fnvvwntila igfewgvalq
 181   hleigkifkg radreaaktr lrefsakagr
 211   qvfkDYVAFP ALTSLSPGAT YRstltanvv
 241   anvirnvwsn avifcghfpd gaekftktdm
 271   igepkGQWYL RQMLGSANFN AGPALRfmsg
 301   nlchqiehhl ypdlpsnrLH EISVRvrevc
 331   drydlpyttg sflvqygktw rtlaklslpd
 361   kylrdnadda petrserMFA GLGPGFAGAD
 391   PVTGRrrglk TAIAAVRgrr rskrmaksvt
 421   epddlaakKL HHHHHH
```

C. flavin and NADPH binding

```
          55   79    120    196    222
2PIA      RtYS grggS GiGITP vycCGP fEsF
consensus r ys  g  s GtG  p y cGp    f
Rv3230c   RsYS egflS GsGITP twaCGP lErF
          109  135   177    257    284
```

FIGURE 4: Primary sequences of Rv3230c and DesA3, including the N- and C-terminal modifications used to add the His_6 tags (shown in uppercase). (A) Primary sequence of Rv3230c with peptides identified by tryptic digest and MALDI-MS analyses indicated with bold type and peptides confirmed by MS/MS analysis indicated with bold and italic type. The experimental and calculated masses of the identified peptides are listed in Table 3. (B) Primary sequence of DesA3 with peptides identified by tryptic digest and MALDI-MS analyses indicated with bold type. The experimental and calculated masses of the identified peptides are listed in Table 3. (C) Residues contributing to flavin and NADPH binding in phthalate dioxygenase reductase, the consensus sequence motif proposed for the ferredoxin $NADP^+$ reductase family (*43*, *58*, *59*), and the corresponding residues in Rv3230c.

transmembrane region in DesA3. This may arise from differences throughout the primary sequences of DesA3 relative to the other homologues but may also arise from incorrect assignment of the cellular location of the C-terminus of DesA3 (*48*). Nevertheless, it is clear from the results of Figure 3B and other work (*5*) that DesA3 is a membrane protein. It has also been previously noted that DesA3 has a number of different amino acid residues near the conserved His motif (*5*). These differences provide tantalizing indications that DesA3 may be distinct from other integral membrane desaturases, which may possibly reflect the electron transfer partners used during catalysis.

Electron Transfer Partners of Membrane Desaturases. The acyl-ACP and acyl-lipid desaturases from the plant plastids

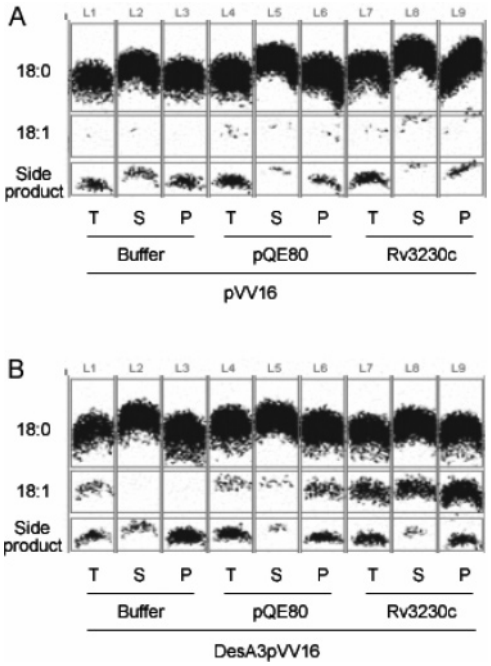

FIGURE 5: Effect of Rv3230c on stearoyl-CoA Δ^9-desaturase activity of DesA3. In this figure, T, S, and P correspond to the total, supernatant, and pellet fractions of the *M. smegmatis* lysate, respectively. The positions of migration of the substrate (18:0), product (18:1), and a side product in the thin-layer chromatography separation are also indicated (see Table 4). (A) Reactions of *M. smegmatis* pVV16 control lysates lacking DesA3. In three separate trials, equal volumes of buffer, an *E. coli* pQE80 control lysate, and an *E. coli* pQE80-Rv3230c containing expressed Rv3230c were studied. (B) Reactions using lysates of *M. smegmatis* pVV16-DesA3 containing DesA3. In three separate trials, equal volumes of buffer, an *E. coli* pQE80 control lysate, and an *E. coli* pQE80-Rv3230c containing expressed Rv3230c were studied. Results from the phosphorimaging of both panels A and B are summarized in Table 4.

use [2Fe-2S] ferredoxin as the electron donor (*18*, *49*−*51*). In vitro, a two-component electron transfer chain can be reconstituted for these enzymes by [2Fe-2S] ferredoxin and ferredoxin reductase (which provides the flavin and NAD binding domains; see Figure 1). In contrast, most other acyl-lipid desaturases of plants and the acyl-CoA desaturases of animals and fungi use the membrane-associated cytochrome b_5 reductase and cytochrome b_5 as a two-component electron transfer chain (*52*−*56*). Furthermore, some desaturases also exist as a fusion with a cytochrome b_5 domain (*57*) and presumably use cytochrome b_5 reductase to initiate electron transfer from NADPH. Other bacterial membrane enzymes such as AlkB and xylene monooxygenase use a specialized rubredoxin (AlkG) and flavoprotein (AlkT) or a multidomain flavin and [2Fe-2S] reductase (XylA) for electron transfer (*27*, *28*).

Properties of Rv3230c. In our search for electron transfer partners for the mycobacterial desaturases, we considered that Rv3230c might be part of an operon along with DesA3. Pfam analysis indicated that Rv3230c would be a fusion of flavin binding, NAD binding, and [2Fe-2S] ferredoxin domains, which would be a suitable composition for a metalloprotein oxidoreductase, albeit one not previously associated with a desaturase enzyme. Neither T4moF, an oxidoreductase with a different domain order, nor the two-component ferredoxin and reductase were able to substitute

Table 3: Diagnostic Peptides of Rv3230c and DesA3 Identified by Tryptic Digestion and MALDI-MS

M_r(expt)[a]	M_r(calc)[b]	Δ[c]	sequence[d]
		Rv3230c	
1100.5409	1100.5992	−0.0583	HPGWHALRK
2406.2249	2406.2583	−0.0334	ITTPLLPDDYLHLANPLWSAR[e]
3658.7488	3658.7837	−0.0349	NQITDVVHLHSAPTAADVMFGAELAALAADHPGYR
2551.1299	2551.1682	−0.0383	SVAADAATSLMDAGEGAGVQLPFGCR[e]
1958.877	1958.9012	−0.0242	MGICQSCVVDLVEGHVR
		DesA3	
730.4927	730.3973	0.0954	ALEVSGR
815.6927	815.4864	0.2063	LLLAGSSR
1181.7927	1181.573	0.2197	YTHNFVHHK
1928.2927	1927.9679	0.3248	DYVAFPALTSLSPGATYR
821.5927	821.4184	0.1743	GQWYLR
1545.9927	1545.7721	0.2206	QMLGSANFNAGPALR
852.6927	852.4817	0.211	LHEISVR
1720.1927	1719.8402	0.3525	MFAGLGPGFAGADPVTGR
700.4927	700.4231	0.0696	TAIAAVR

[a] Experimental mass determined by MALDI-MS. [b] Calculated mass from the primary sequence. [c] Difference between the experimental and calculated masses. [d] Sequence of the identified peptide deduced from the combination of tryptic digest and mass results. The positions of these peptides in either Rv3230c or DesA3 are shown in Figure 4. [e] The primary sequence of these peptides was confirmed by MS/MS analysis.

Table 4: Percentage of the Total Phosphorimager Signal[a] Determined for the Different Lanes Shown in Figure 5

	Lanes from Figure 4								
	L1	L2	L3	L4	L5	L6	L7	L8	L9
M. smegmatis fraction[b]	total	soluble	pellet	total	soluble	pellet	total	soluble	pellet
E. coli pQE80 lysate	−	−	−	+	+	+	−	−	−
E. coli pQE80-Rv3230c lysate	−	−	−	−	−	−	+	+	+
M. smegmatis pVV16[c]									
% 18:0	82%	91%	86%	84%	95%	91%	84%	95%	93%
% 18:1	6%	3%	3%	4%	3%	4%	4%	3%	3%
% side product[d]	12%	6%	11%	12%	2%	5%	12%	2%	4%
M. smegmatis pVV16-DesA3[e]									
% 18:0	74%	91%	74%	77%	94%	83%	66%	83%	63%
% 18:1	13%	3%	4%	7%	4%	9%	20%	14%	28%
% side product	13%	6%	22%	16%	2%	8%	14%	3%	9%
fold increase in 18:1[f]	2.2	1.0	1.3	1.8	1.3	2.5	5.0	4.7	9.3

[a] Samples were analyzed by phosphorimaging as described in Experimental Procedures. [b] The subcellular fraction of *M. smegmatis* used in the experiment: total cell lysate, soluble fraction, or pellet fraction prepared as described in Experimental Procedures. [c] Control studies using *M. smegmatis* pVV16 not able to express DesA3. [d] This pattern of separation of radiolabeled 18:0 from total cellular lipids has been observed in other studies (e.g., see Figure 3 of ref *31*). Our MALDI and GC−MS analysis of the side product obtained from unlabeled reactions showed that this band contained a mixture of 16:0, 16:1, 18:0, and 18:1 fatty acids, with 16:1 being predominant, 16:0 and 18:0 present in small amounts, and 18:1 present in a trace amount. Among these products, only 18:0 and 18:1 would be detected by the radioisotope method. GC−MS analysis of the dimethyl disulfide-treated, unlabeled side product showed that the abundant 16:1 was desaturated at the Δ^7 position, while the trace amount of 18:1 failed to yield a diagnostic product. On the basis of the comigration with Δ^7-16:1, it is plausible that the radiolabeled side product is Δ^7-18:1. [e] Desaturase reaction studies using *M. smegmatis* pVV16-DesA3 expressing DesA3. [f] The fold increase in the level of 18:1 production relative to the comparable control studies.

for Rv3230c in catalytic assays (Figure 1). Thus, Rv3230c has specificity for the reaction with DesA3.

The sequence of Rv3230c is only 23% identical with that of phthalate dioxygenase reductase. Nevertheless, the X-ray structure of phthalate dioxygenase reductase provided an excellent structural homology model for Rv3230c (see panels A and B of Figure 7, respectively). The homology model had an *E* value of 2.97×10^{-5}, where *E* values smaller than 0.05 indicate an increasingly high probability for the match between sequence and target structure. In the threaded structure, the first 58 residues of Rv3230c were not modeled to the smaller dioxygenase reductase. This unmatched region has amphipathic character, with a predicted short hydrophobic region immediately preceding the start of the flavin binding domain (white spheres in Figure 7B). Overall, the remainder of the Rv3230c model closely matched the three-domain structure of phthalate dioxygenase reductase, including conserved residues making contact with the flavin cofactor and the NAD(P)H binding domain (*43*, *58*, *59*; summarized in Figure 3C) and the spacing of the Cys ligands to the [2Fe-2S] center (e.g., Cys333, Cys338, Cys341, and Cys368 of Rv3230c and Cys272, Cys277, Cys280, and Cys308 of 2PIA). Of note, Phe225 from phthalate dioxygenase reductase has been proposed to have configurational flexibility for the promotion of nicotinamide flavin stacking (*42*), and this residue is conserved in Rv3230c as Phe287.

Only a few residue positions exhibited deviations of the experimental and predicted backbone atoms of >1 Å (orange tubes in Figure 7B). One of the variable loops in Rv3230c was predicted to precede the Arg55−Ser58 sequence that contributes contacts to N5 of FMN in phthalate dioxygenase reductase. Another of the variable loops in Rv3230c was also predicted to be near the putative flavin binding site. This loop included an insertion of five residues, perhaps corresponding to a difference that might accommodate FAD binding suggested in Rv3230c instead of FMN found in

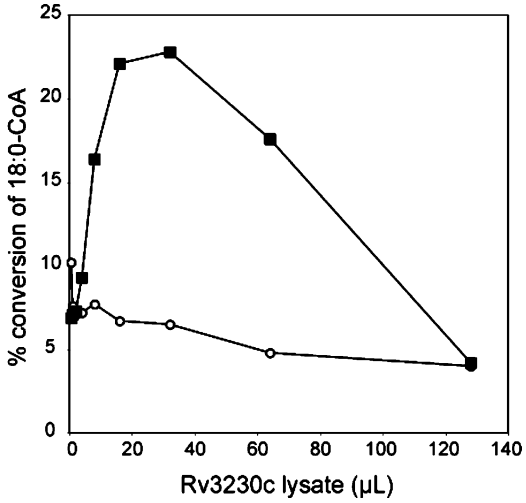

FIGURE 6: Dependence of DesA3 activity upon addition of increasing amounts of lysate containing Rv3230c. (■) Addition of lysates made from *E. coli* pQE80-Rv3230c (0−128 μL of a lysate with a total protein concentration of 10 mg/mL). The percentage conversion of 18:0-CoA to 18:1-CoA was determined by the same fixed time assay that was used for the experiments depicted in Figure 5 and Table 4, which contained 15 μL of *E. coli* pQE80-Rv3230c lysate. (○) Addition of lysate made from *E. coli* pQE80. The protein concentrations of the pQE80 and pQE80-Rv3230c lysates were normalized before the start of the experiment.

phthalate dioxygenase reductase. Two of the other variable loops were on the surface of the [2Fe-2S] domain nearest the interface with the flavin binding site. One noticeable difference between the threaded structure of Rv3230c and phthalate dioxygenase reductase was the predicted number of surface Arg and Lys residues on Rv3230c, which contribute to the elevated pI of 9.4. Since Rv3230c reacts with an integral membrane protein, a net positive surface charge may facilitate interactions with a negatively charged phospholipid membrane.

Comparison with Other Mycobacterial Desaturases. M. smegmatis has several DesA3 homologues on the basis of sequence annotations. Constitutive expression of one of these homologues might have contributed to the low level of background accumulation of 18:1-CoA observed in control assays. However, since exogenous unsaturated fatty acids often reduce the level of expression of stearoyl-CoA desaturases (*60*−*63*), the presence of oleic acid in the growth medium may have also substantially inhibited expression of these endogenous desaturases. By comparison, the heterologous expression of *M. tuberculosis* DesA3 from pVV16 was under the control of the hsp60 promoter and would likely not be directly affected by medium composition.

As defined here, the DesA3 complex from *M. tuberculosis* is composed of a soluble reductase and a membrane-bound desaturase. This composition is distinct from that of an entirely soluble *cis*-Δ^{15} 24:0-CoA desaturase system reported from *M. smegmatis* (*64*). This previously described three-protein complex consisted of an NADPH oxidase, a ferredoxin-containing fraction, and a terminal desaturase that had low reactivity for 18:0-CoA.

A stearoyl-CoA Δ^9-desaturase was also reported from *Mycobacterium phlei* (*65*, *66*). This enzyme was a three-component particulate system consisting of an FAD-requiring NADPH-cytochrome *c* reductase, an intermediate carrier of unknown nature, and a cyanide-sensitive terminal oxidase. The complex from *M. tuberculosis* presented here is notably similar to this *M. phlei* complex, perhaps corresponding to the FAD-requiring reductase and the terminal oxidase. The nature of the intermediate carrier, if indeed required for the Rv3230c and DesA3 complex, is not known. In principle, the *M. smegmatis* lysate might provide other complementary proteins required for function of the *M. tuberculosis* DesA3 complex. We considered whether five other ferredoxins (Rv0763c, Rv1177, Rv1786, Rv2007c, and Rv3503c) present in the *M. tuberculosis* H37Rv genome might also be part of a DesA3 complex. However, since none of the genes for these ferredoxins are located near *desA3*, and since the available gene expression results do not reveal a correlation,

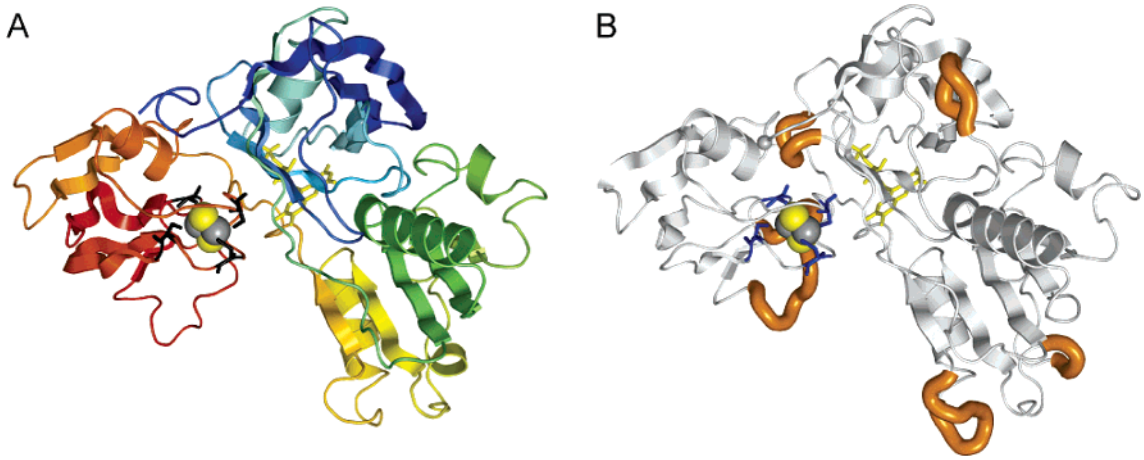

FIGURE 7: Structural relationship in the multidomain oxidoreductase subfamily defined by phthalate dioxygenase reductase. (A) X-ray structure of phthalate dioxygenase reductase [2PIA (*42*)]. The cartoon representation of the protein backbone is shown as a color gradient from blue at the N-terminus to red at the C-terminus. The flavin binding domain is colored predominantly blue, the NADPH binding domain green and yellow, and the [2Fe-2S] domain orange and red. The positions of conserved Cys ligands to the [2Fe-2S] center are shown as black sticks; the [2Fe-2S] center is shown as gray and yellow spheres, and the bound FMN is shown as yellow sticks. (B) A predicted structure of Rv3230c determined by molecular threading of the Rv3230c primary sequence onto the X-ray structure of phthalate dioxygenase reductase. The first modeled atom at the N-terminus, Ala58 N, is shown as a white sphere. The predicted positions of loops that deviate from the positions in 2PIA are shown as orange tubes. The positions of conserved Cys residues that may ligate the [2Fe-2S] center are shown as blue sticks. In the Rv3230c threaded structure, the positions of the [2Fe-2S] center and the isoalloxazine ring were transferred from the aligned phthalate dioxygenase reductase structure for reference only.

the role of these other ferredoxins in the DesA3 complex is not easily ascertained.

Catalysis by the DesA3 Complex. Our measurements using different combinations of soluble and pellet fractions without Rv3230c had no significant desaturase activity, as previously observed using *M. bovis* BCG lysate (*5*). We found that *E. coli* control lysates could provide a weak stimulation of 18:0-CoA desaturation in *M. smegmatis* lysates expressing DesA3. This activity did not increase as more of the control lysate was added (Figure 6), suggesting nonspecific interactions of endogenous *E. coli* proteins. In contrast, 18:0-CoA desaturase activity was readily detected when either total or pellet fractions prepared from *M. smegmatis* expressing DesA3 were mixed with a lysate containing Rv3230c. The stimulation of the DesA3 reaction by the Rv3230c lysate exhibited apparent saturation behavior but also became inhibitory at higher concentrations. The saturation behavior is typical when one protein of an enzyme complex is treated as a varied substrate in standard steady-state kinetic analysis (*67*). Moreover, the addition of excess oxidoreductase may also lead to enzyme inhibition due to an uncoupled adventitious oxidation of NAD(P)H (*34*, *35*), which apparently occurred when large amounts of the Rv3230c lysate were used.

Summary. These results demonstrate that Rv3230c is a biologically relevant electron transfer partner for DesA3, providing biochemical verification of the genome annotation, operon prediction, and expression array studies of others (*8*, *9*). Knowledge of the individual protein components of this complex provides a basis for a more detailed examination of the properties of this plausible mycobacterial drug target.

ACKNOWLEDGMENT

We acknowledge the websites provided by the TB Protein Structure Initiative (http://www.doe-mbi.ucla.edu/TB/ and http://www.doe-mbi.ucla.edu/~strong/map/) and the expression array data obtained from the cited references.

REFERENCES

1. Dye, C., Scheele, S., Dolin, P., Pathania, V., and Raviglione, M. C. (1999) Consensus statement. Global burden of tuberculosis: Estimated incidence, prevalence, and mortality by country. WHO Global Surveillance and Monitoring Project, *J. Am. Med. Assoc. 282*, 677−86.
2. Centers for Disease Control and Prevention (2004) *TB elimination: Now is time!* Centers for Disease Control and Prevention, Atlanta, GA.
3. Young, D. B., and Cole, S. T. (1993) Leprosy, tuberculosis, and the new genetics, *J. Bacteriol. 175*, 1−6.
4. Bloom, B. R., and Murray, C. J. (1992) Tuberculosis: Commentary on a reemergent killer, *Science 257*, 1055−64.
5. Phetsuksiri, B., Jackson, M., Scherman, H., McNeil, M., Besra, G. S., Baulard, A. R., Slayden, R. A., DeBarber, A. E., Barry, C. E., III, Baird, M. S., Crick, D. C., and Brennan, P. J. (2003) Unique mechanism of action of the thiourea drug isoxyl on *Mycobacterium tuberculosis*, *J. Biol. Chem. 278*, 53123−30.
6. Cole, S. T., Brosch, R., and Parkhill, J. (1998) Deciphering the biology of *Mycobacterium tuberculosis* from the complete genome sequence, *Nature 393*, 537−44.
7. Marmiesse, M., Brodin, P., Buchrieser, C., Gutierrez, C., Simoes, N., Vincent, V., Glaser, P., Cole, S. T., and Brosch, R. (2004) Macro-array and bioinformatic analyses reveal mycobacterial 'core' genes, variation in the ESAT-6 gene family and new phylogenetic markers for the *Mycobacterium tuberculosis* complex, *Microbiology 150*, 483−96.
8. Betts, J. C., Lukey, P. T., Robb, L. C., McAdam, R. A., and Duncan, K. (2002) Evaluation of a nutrient starvation model of *Mycobacterium tuberculosis* persistence by gene and protein expression profiling, *Mol. Microbiol. 43*, 717−31.
9. Schnappinger, D., Ehrt, S., Voskuil, M. I., Liu, Y., Mangan, J. A., Monahan, I. M., Dolganov, G., Efron, B., Butcher, P. D., Nathan, C., and Schoolnik, G. K. (2003) Transcriptional adaptation of *Mycobacterium tuberculosis* within macrophages: Insights into the phagosomal environment, *J. Exp. Med. 198*, 693−704.
10. Parish, T., Smith, D. A., Roberts, G., Betts, J., and Stoker, N. G. (2003) The senX3-regX3 two-component regulatory system of *Mycobacterium tuberculosis* is required for virulence, *Microbiology 149*, 1423−35.
11. Voskuil, M. I., Visconti, K. C., and Schoolnik, G. K. (2004) *Mycobacterium tuberculosis* gene expression during adaptation to stationary phase and low-oxygen dormancy, *Tuberculosis 84*, 218−27.
12. Goulding, C. W., Apostol, M., Anderson, D. H., Gill, H. S., Smith, C. V., Kuo, M. R., Yang, J. K., Waldo, G. S., Suh, S. W., Chauhan, R., Kale, A., Bachhawat, N., Mande, S. C., Johnston, J. M., Lott, J. S., Baker, E. N., Arcus, V. L., Leys, D., McLean, K. J., Munro, A. W., Berendzen, J., Sharma, V., Park, M. S., Eisenberg, D., Sacchettini, J., Alber, T., Rupp, B., Jacobs, W., Jr., and Terwilliger, T. C. (2002) The TB structural genomics consortium: Providing a structural foundation for drug discovery, *Curr. Drug Targets Infect. Disord. 2*, 121−41.
13. Barry, C. E., III, Lee, R. E., Mdluli, K., Sampson, A. E., Schroeder, B. G., Slayden, R. A., and Yuan, Y. (1998) Mycolic acids: Structure, biosynthesis and physiological funcations, *Prog. Lipid Res. 37*, 143−79.
14. Glickman, M. S., and Jacobs, W. R., Jr. (2001) Microbial pathogenesis of *Mycobacterium tuberculosis*: Dawn of a discipline, *Cell 104*, 477−85.
15. Brennan, P. J., and Nikaido, H. (1995) The envelope of mycobacteria, *Annu. Rev. Biochem. 64*, 29−63.
16. Takayama, K., Wang, C., and Besra, G. S. (2005) Pathway to synthesis and processing of mycolic acids in *Mycobacterium tuberculosis*, *Clin. Microbiol. Rev. 18*, 81−101.
17. Shanklin, J., and Somerville, C. (1991) Stearoyl-acyl-carrier-protein desaturase from higher plants is structurally unrelated to the animal and fungal homologs, *Proc. Natl. Acad. Sci. U.S.A. 88*, 2510−4.
18. Fox, B. G., Lyle, K. S., and Rogge, C. E. (2004) Reactions of the diiron enzyme stearoyl-acyl carrier protein desaturase, *Acc. Chem. Res. 37*, 421−9.
19. Dyer, D. H., Lyle, K. S., Rayment, I., and Fox, B. G. (2005) X-ray structure of putative acyl-ACP desaturase DesA2 from *Mycobacterium tuberculosis* H37Rv, *Protein Sci. 14*, 1508−17.
20. Lim, E. M., Rauzier, J., Timm, J., Torrea, G., Murray, A., Gicquel, B., and Portnoi, D. (1995) Identification of *Mycobacterium tuberculosis* DNA sequences encoding exported proteins by using phoA gene fusions, *J. Bacteriol. 177*, 59−65.
21. Jackson, M., Portnoi, D., Catheline, D., Dumail, L., Rauzier, J., Legrand, P., and Gicquel, B. (1997) *Mycobacterium tuberculosis* Des protein: An immunodominant target for the humoral response of tuberculous patients, *Infect. Immun. 65*, 2883−9.
22. Downing, K. J., McAdam, R. A., and Mizrahi, V. (1999) *Staphylococcus aureus* nuclease is a useful secretion reporter for mycobacteria, *Gene 239*, 293−9.
23. Walker, R. W., Barakat, H., and Hung, J. G. (1970) The positional distribution of fatty acids in the phospholipids and triglycerides of *Mycobacterium smegmatis* and *M. bovis* BCG, *Lipids 5*, 684−91.
24. Hung, J. G., and Walker, R. W. (1970) Unsaturated fatty acids of Mycobacteria, *Lipids 5*, 720−2.
25. Okuyama, H., Kankura, T., and Nojima, S. (1967) Positional distribution of fatty acids in phospholipids from Mycobacteria, *J. Biochem. 61*, 732−7.
26. Shanklin, J., Whittle, E., and Fox, B. G. (1994) Eight histidine residues are catalytically essential in a membrane-associated iron enzyme, stearoyl-CoA desaturase, and are conserved in alkane hydroxylase and xylene monooxygenase, *Biochemistry 33*, 12787−94.
27. Kok, M., Oldenhuis, R., van der Linden, M. P., Raatjes, P., Kingma, J., van Lelyveld, P. H., and Witholt, B. (1989) The *Pseudomonas oleovorans* alkane hydroxylase gene. Sequence and expression, *J. Biol. Chem. 264*, 5435−41.
28. Suzuki, M., Hayakawa, T., Shaw, J. P., Rekik, M., and Harayama, S. (1991) Primary structure of xylene monooxygenase: Similarities to and differences from the alkane hydroxylation system, *J. Bacteriol. 173*, 1690−5.

29. Jackson, M., Crick, D. C., and Brennan, P. J. (2000) Phosphatidylinositol is an essential phospholipid of mycobacteria, *J. Biol. Chem. 275*, 30092−9.
30. Sreenath, H. K., Bingman, C. A., Buchan, B. W., Seder, K. D., Burns, B. T., Geetha, H. V., Jeon, W. B., Vojtik, F. C., Aceti, D. J., Frederick, R. O., Phillips, G. N., Jr., and Fox, B. G. (2005) Protocols for production of selenomethionine-labeled proteins in 2-L polyethylene terephthalate bottles using auto-induction medium, *Protein Expression Purif. 40*, 256−67.
31. Miyazaki, M., Jacobson, M. J., Man, W. C., Cohen, P., Asilmaz, E., Friedman, J. M., and Ntambi, J. M. (2003) Identification and characterization of murine SCD4, a novel heart-specific stearoyl-CoA desaturase isoform regulated by leptin and dietary factors, *J. Biol. Chem. 278*, 33904−11.
32. Haas, J. A., and Fox, B. G. (1999) Role of hydrophobic partitioning in substrate selectivity and turnover of the *Ricinus communis* stearoyl acyl carrier protein Δ^9 desaturase, *Biochemistry 38*, 12833−40.
33. Buser, H. R., Arn, H., Guerin, P., and Rauscher, S. (1983) Determination of double bond position in mono-unsaturated acetates by mass spectrometry of dimethyl disulfide adducts, *Anal. Chem. 55*, 818−22.
34. Pikus, J. D., Studts, J. M., Achim, C., Kauffmann, K. E., Munck, E., Steffan, R. J., McClay, K., and Fox, B. G. (1996) Recombinant toluene-4-monooxygenase: Catalytic and Mossbauer studies of the purified diiron and Rieske components of a four-protein complex, *Biochemistry 35*, 9106−19.
35. Mitchell, K. H., Studts, J. M., and Fox, B. G. (2002) Combined participation of hydroxylase active site residues and effector protein binding in a para to ortho modulation of toluene 4-monooxygenase regiospecificity, *Biochemistry 41*, 3176−88.
36. Ermolaeva, M. D., White, O., and Salzberg, S. L. (2001) Prediction of operons in microbial genomes, *Nucleic Acids Res. 29*, 1216−21.
37. Schwede, T., Kopp, J., Guex, N., and Peitsch, M. C. (2003) SWISS-MODEL: An automated protein homology-modeling server, *Nucleic Acids Res. 31*, 3381−5.
38. Kyte, J., and Doolittle, R. F. (1982) A simple method for displaying the hydropathic character of a protein, *J. Mol. Biol. 157*, 105−32.
39. Krogh, A., Larsson, B., von Heijne, G., and Sonnhammer, E. L. (2001) Predicting transmembrane protein topology with a hidden Markov model: Application to complete genomes, *J. Mol. Biol. 305*, 567−80.
40. Sonnhammer, E. L., von Heijne, G., and Krogh, A. (1998) A hidden Markov model for predicting transmembrane helices in protein sequences, *Proc.—Int. Conf. Intell. Syst. Mol. Biol., 6th*, 175−82.
41. Higgins, D. G., Thompson, J. D., and Gibson, T. J. (1996) Using CLUSTAL for multiple sequence alignments, *Methods Enzymol. 266*, 383−402.
42. Correll, C. C., Batie, C. J., Ballou, D. P., and Ludwig, M. L. (1992) Phthalate dioxygenase reductase: A modular structure for electron transfer from pyridine nucleotides to [2Fe-2S], *Science 258*, 1604−10.
43. Neidle, E. L., Hartnett, C., Ornston, L. N., Bairoch, A., Rekik, M., and Harayama, S. (1991) Nucleotide sequences of the *Acinetobacter calcoaceticus* benABC genes for benzoate 1,2-dioxygenase reveal evolutionary relationships among multicomponent oxygenases, *J. Bacteriol. 173*, 5385−95.
44. Kauppi, B., Lee, K., Carredano, E., Parales, R. E., Gibson, D. T., Eklund, H., and Ramaswamy, S. (1998) Structure of an aromatic-ring-hydroxylating dioxygenase-naphthalene 1,2-dioxygenase, *Structure 6*, 571−86.
45. Ballou, D., and Batie, C. (1988) Phthalate oxygenase, a Rieske iron-sulfur protein from *Pseudomonas cepacia*, *Prog. Clin. Biol. Res. 274*, 211−26.
46. Lipscomb, J. D. (1994) Biochemistry of the soluble methane monooxygenase, *Annu. Rev. Microbiol. 48*, 371−99.
47. Karlsson, A., Beharry, Z. M., Matthew Eby, D., Coulter, E. D., Neidle, E. L., Kurtz, D. M., Jr., Eklund, H., and Ramaswamy, S. (2002) X-ray crystal structure of benzoate 1,2-dioxygenase reductase from *Acinetobacter* sp. strain ADP1, *J. Mol. Biol. 318*, 261−72.
48. Melen, K., Krogh, A., and von Heijne, G. (2003) Reliability measures for membrane protein topology prediction algorithms, *J. Mol. Biol. 327*, 735−44.
49. McKeon, T. A., and Stumpf, P. K. (1982) Purification and characterization of the stearoyl-acyl carrier protein desaturase and the acyl-acyl carrier protein thioesterase from maturing seeds of safflower, *J. Biol. Chem. 257*, 12141−7.
50. Schmidt, H., and Heinz, E. (1990) Desaturation of oleoyl groups in envelope membranes from spinach chloroplasts, *Proc. Natl. Acad. Sci. U.S.A. 87*, 9477−80.
51. Schmidt, H., and Heinz, E. (1990) Involvement of ferredoxin in desaturation of lipid-bound oleate in chloroplasts, *Plant Physiol. 94*, 214−20.
52. Smith, M. A., Cross, A. R., Jones, O. T., Griffiths, W. T., Stymne, S., and Stobart, K. (1990) Electron-transport components of the 1-acyl-2-oleoyl-sn-glycero-3-phosphocholine Δ12-desaturase (Δ12-desaturase) in microsomal preparations from developing safflower (*Carthamus tinctorius* L.) cotyledons, *Biochem. J. 272*, 23−9.
53. Kearns, E. V., Hugly, S., and Somerville, C. R. (1991) The role of cytochrome b5 in Δ12 desaturation of oleic acid by microsomes of safflower (*Carthamus tinctorius* L.), *Arch. Biochem. Biophys. 284*, 431−6.
54. Dailey, H. A., and Strittmatter, P. (1980) Characterization of the interaction of amphipathic cytochrome b5 with stearyl coenzyme A desaturase and NADPH:cytochrome P-450 reductase, *J. Biol. Chem. 255*, 5184−9.
55. Mitchell, A. G., and Martin, C. E. (1995) A novel cytochrome b5-like domain is linked to the carboxyl terminus of the *Saccharomyces cerevisiae* Δ-9 fatty acid desaturase, *J. Biol. Chem. 270*, 29766−72.
56. Jeffcoat, R., Brawn, P. R., Safford, R., and James, A. T. (1977) Properties of rat liver microsomal stearoyl-coenzyme A desaturase, *Biochem. J. 161*, 431−7.
57. Sperling, P., Ternes, P., Zank, T. K., and Heinz, E. (2003) The evolution of desaturases, *Prostaglandins, Leukotrienes Essent. Fatty Acids 68*, 73−95.
58. Karplus, P. A., Daniels, M. J., and Herriott, J. R. (1991) Atomic structure of ferredoxin-$NADP^+$ reductase: Prototype for a structurally novel flavoenzyme family, *Science 251*, 60−6.
59. Andrews, S. C., Shipley, D., Keen, J. N., Findlay, J. B., Harrison, P. M., and Guest, J. R. (1992) The haemoglobin-like protein (HMP) of *Escherichia coli* has ferrisiderophore reductase activity and its C-terminal domain shares homology with ferredoxin $NADP^+$ reductases, *FEBS Lett. 302*, 247−52.
60. Mercuri, O., Peluffo, R. O., and de Tomas, M. E. (1974) Effect of different diets on the Δ9-desaturase activity of normal and diabetic rats, *Biochim. Biophys. Acta 369*, 264−8.
61. Bossie, M. A., and Martin, C. E. (1989) Nutritional regulation of yeast Δ-9 fatty acid desaturase activity, *J. Bacteriol. 171*, 6409−13.
62. McDonough, V. M., Stukey, J. E., and Martin, C. E. (1992) Specificity of unsaturated fatty acid-regulated expression of the *Saccharomyces cerevisiae* OLE1 gene, *J. Biol. Chem. 267*, 5931−6.
63. Tebbey, P. W., and Buttke, T. M. (1992) Arachidonic acid regulates unsaturated fatty acid synthesis in lymphocytes by inhibiting stearoyl-CoA desaturase gene expression, *Biochim. Biophys. Acta 1171*, 27−34.
64. Kikuchi, S., and Kusaka, T. (1986) Isolation and partial characterization of a very long-chain fatty acid desaturation system from the cytosol of *Mycobacterium smegmatis*, *J. Biochem. 99*, 723−31.
65. Kashiwabara, Y., Nakagawa, H., Matsuki, G., and Sato, R. (1975) Effect of metal ions in the culture medium on the stearoyl-coenzyme A desaturase activity of *Mycobacterium phlei*, *J. Biochem. 78*, 803−10.
66. Kashiwabara, Y., and Sato, R. (1973) Electron transfer mechanism involved in stearoyl-coenzyme A desaturation by particulate fraction of *Mycobacterium phlei*, *J. Biochem. 74*, 405−13.
67. Fox, B. G., Liu, Y., Dege, J. E., and Lipscomb, J. D. (1991) Complex formation between the protein components of methane monooxygenase from *Methylosinus trichosporium* OB3b. Identification of sites of component interaction, *J. Biol. Chem. 266*, 540−50.
68. Snapper, S. B., Melton, R. E., Mustafa, S., Kieser, T., and Jacobs, W. R., Jr. (1990) Isolation and characterization of efficient plasmid transformation mutants of *Mycobacterium smegmatis*, *Mol. Microbiol. 4*, 1911−9.

BI0615285